Astronomy & Astrophysics

Rotation period and magnetic field morphology
of the white dwarf WD 0009+501

G. Valyavin[1,2], S. Bagnulo[3], D. Monin[4], S. Fabrika[2], B.-C. Lee[1], G. Galazutdinov[1,2], G. A. Wade[5], and T. Burlakova[2]

[1] Korea Astronomy and Space Science institute, 61-1, Whaam-Dong, Youseong-Gu, Taejeon 305-348, Republic of Korea
   e-mail: gendoz@boao.re.kr
[2] Special Astrophysical Observatory, Russian Academy of Sciences, Nizhnii Arkhyz, Karachai Cherkess Republic
   357147, Russia
[3] European Southern Observatory, Alonso de Cordova 3107, Santiago, Chile
[4] Département de Physique et d'Astronomie, Université de Moncton, Moncton, NB, E1A 3E9, Canada
[5] Department of Physics, Royal Military College of Canada, PO Box 17000 Stn "FORCES", Kingston, Ontario,
   K7K 7B4, Canada

Abstract. We present new spectropolarimetric observations of the weak-field magnetic white dwarf WD 0009+501. From these data we estimate that the star's longitudinal magnetic field varies with the rotation phase from about -120 kG to about $+50$ kG, and that the surface magnetic field varies from about 150 kG to about 300 kG. Earlier estimates of the stellar rotation period are revised anew, and we find that the most probable period is about 8 h. We have attempted to recover the star's magnetic morphology by modelling the available magnetic observables, assuming that the field is described by the superposition of a dipole and a quadrupole. According to the best-fit model, the inclination of the rotation axis with respect to the line of sight is $i = 60° \pm 20°$, and the angle between the rotation axis and the dipolar axis is $\beta = 111° \pm 17°$. The dipole strength at the pole is about 340 kG, and the quadrupolar strength is about 300 kG.

Key words. stars: white dwarfs – stars: magnetic fields – stars: rotation – stars: individual: WD 0009+501

1. Introduction

It is generally assumed that magnetic white dwarfs are the descendants of magnetic Ap/Bp stars. This assumption, if true, suggests that magnetic white dwarfs, as relics of stellar cores, are unique indicators revealing remnants of internal fields of intermediate-mass stars. Therefore, spectropolarimetric investigation of magnetic white dwarfs is of fundamental importance for understanding the origin and evolution of global stellar magnetic fields. Knowing white dwarf magnetic field geometries, strengths and rotation periods, one may restrict assumptions in theories of the evolution of intermediate mass stars. For instance, the rotation periods and surface magnetic fields of white dwarfs could be used to find the angular momentum and magnetic flux lost by a star during formation of the degenerate core and associated mass loss. The distribution of white dwarf magnetic field strengths could yield information about whether magnetic white dwarfs represent an independent class of strongly-magnetic degerate stars, or if they are those objects with the strongest fields in a continuous distribution of field strengths (Angel et al. 1981; Wickramasinghe & Ferrario 2000, 2005).

While the theory of white dwarf magnetic fields has been developing quite successfully (for instance Wendell et al. 1987; Muslimov et al. 1995), observational data are still required, especially in a low-field regime (Schmidt & Smith 1994, 1995; Valyavin et al. 2003; Liebert et al. 2003). Presently, only a few white dwarfs with the fields below 1 MG are known (Aznar Cuadrado et al. 2004, and references therein). Their rotation and magnetic field geometries are poorly studied, although some progresses have been made recently with the work by Maxted et al. (2000) on WD 1953-011, a white dwarf characterised by one of the weakest measured fields. Maxted et al. (2000) discovered that the magnetic morphology of WD 1953-011 is dominated by a strong non-dipolar component ($\sim$500 kG; see also Wade et al. 2004). This result has shown that the interpretation of the spectra of sub-megaGauss magnetic white dwarfs which is a crucial point for understading the processes of stellar magnetic field evolution. In order to continue the discussion, here we present a study of the rotation period and the magnetic morphology of another weak-field white dwarf: WD 0009+501.

WD 0009+501 (=GJ 1004) was first discovered as a low field magnetic degenerate by Schmidt & Smith (1994). In twelve observations obtained during four observing nights,

they found variations of the longitudinal magnetic field over the range $B_1 = -100 \div +9$ kG with error bars $\sigma(B_1) = 8 \div 15$ kG. Assuming the magnetic field varies because of the star's rotation, they found the probable period to be between 2 and 20 h. Power spectrum analysis displayed various periods in this region with some preference for shorter periods. No variation of the magnetic field was found in a pair of spectra separated by 12 min, but significant difference was detected in observations separated by 5 h. Field variation of about 100 kG was detected.

More recently (Fabrika et al. 2003) we repeated Zeeman observations of this white dwarf. The series of observations consisted of 21 consecutive Zeeman spectra taken with 5- and 10-min exposures. These measurements confirmed the presence of a varying magnetic field in WD 0009+501. The rotation period was estimated about 2 h.

To further study the magnetic field configuration we obtained additional observations at the 6 m Russian telescope BTA, and performed new determinations of the mean longitudinal field, mean field modulus and mean asymmetry of the longitudinal field multiplied by $v_e \sin i$ (crossover). In fact, we found that our new observations are not consistent with the earlier estimate of the rotation period. In this paper we present a new determination of the rotation period and a magnetic model consistent with all determinations of the magnetic observables.

2. New observations and data reduction

The observations were carried out in the course of six nights from December 29, 2003 to January 3, 2004 with the prime focus spectrograph-polarimeter UAGS of the 6 m telescope ($R \sim 2000$). The instrument and observational technique are described in detail by Afanasiev et al. (1995) and by Naydenov et al. (2002). The spectropolarimeter is a standard spectrograph equipped with a rotatable quarter-wave plate and a beam-splitting analyzer. Each CCD image contains two spectra of opposite circular polarizations split by the analyzer. A circular polarization observation consists of a series of paired exposures obtained at two orthogonal orientations of the waveplate (the modulation technique, similar to that described by Schmidt & Smith 1994). We estimated a priori that the time-scale for the variability of the observed magnetic field could be as short as a few minutes. For this reason, but also to limit the parasitic influence of atmospheric sincillation, we decided to set the integration time of each exposure to 150 s.

The reduction of the CCD images were carried out using the image processing packages MIDAS (context "LONG" for long-slit spectrographs). The applied procedures were mostly standard including the following steps: cosmic ray hits removing, electronic bias substraction, flat-fielding, 2D wavelength calibration, sky background substraction, spectrum extraction. Finally we obtained a series of pairs of left and right circular polarized spectra that were used to search for the rotation period as described in Sect. 3.

3. Period determination

For the search of the star's rotation period we used the determinations of disk-averaged longitudinal component of the magnetic field B_1 obtained from our spectra. Longitudinal field measurements were first obtained via analysis of the displacement between the positions of Hα in the spectra of opposite circular polarizations. For the determination of the line profile displacement we used a technique based on estimate of the autocorrelation function of Zeeman shifted spectral features using the discrete Fourier transform (Scargle 1989). This technique appears to be relatively insensitive to uncertainties in the continuum determination (Klochkova et al. 1996). For the determination of the mean longitudinal field we used the formula:

$$\Delta\lambda = \lambda_R - \lambda_L = 9.34 \times 10^{-13} g_{\text{eff}} B_1 \lambda^2 \tag{1}$$

where g_{eff}-effective Lande factor, B_1-longitudinal magnetic field and λ-wavelength (for more detail see Monin et al. 2002, and references therein). A preliminary inspections to the series of longitudinal field values allowed us to rule out a variability time-scale shorter than 600 s. Hence we decided to consider a series of longitudinal field determinations where each individual value is obtained from the weighted average of four (consecutive) points. We obtained a series of field determinations where each point correponds to 600 s exposure[1]. These values are listed in Table 1, where we also present reprocessed and averaged data (JD = 2 451 423 at the table) that were obtained earlier with spectrograph SP-124 of the 6-m telescope (described by Fabrika et al. 2003).

To determine the rotation period we applied the Lafler-Kinman method (Lafler & Kinman 1965), as modified by Goransky (2004). In case of non-uniformly sampled and highly noisy data, this method leads to more accurate results than the traditional Fourier power spectrum analysis.

Analysis of the power spectrum of the data revealed a strong signal indicating a probable period ranging from 5 h to 1 day (Fig. 1). This is consistent with the period range $2 < P < 20$ h suggested by Schmidt & Smith (1994). A detailed study of the periodogram showed that the most significant sinusoidal signal corresponds to about 8 h ($P = 8$ h ± 5 min). Other peaks are present around 12 and 16 h. However, the longitudinal field curves obtained using a rotation period of 12 h or 16 h show a bimodal structure that cannot be interpreted in terms of a simple low-order multipolar expansion of the magnetic field. To test the reliability of the 8 h period we performed a "spectral cleaning" of the periodogram as described by Terebizh (1992). We fit and extracted a sinusoidal function of a 8 h period from the observed data, and carried out the periodogram analysis for the residual data. If the tested period is correct, we expect the residual periodogram be nearly "white noise" structure (Terebizh 1992). If real signal has multi-frequency nature, the spectral cleaning needs to be carried out iteratively using multi-frequency trial harmonic functions. Our analysis indicates that the best result is obtained with the 8 h period (the lower panel in Fig. 1).

---

[1] With two exceptions: because of weather conditions, in two different cases we had to co-add spectra for a total of 25 and 30 m, respectively; see Table 1.

Table 1. Determinations of mean longitudinal field obtained as explained in Sect. 2. Column 1 is the Julian Date, Col. 2 is the equivalent exposure time, Col. 3 is the mean longitudinal magnetic field (in kG), Col. 4 is the associated error bar (in kG).

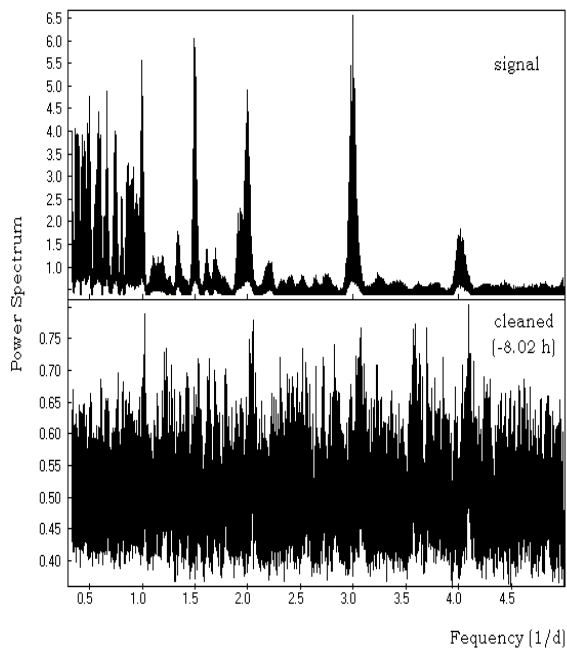| JD – 2 400 000	Exp (s)	B_l (kG)	σ (kG)	JD – 2 400 000	Exp (s)	B_l (kG)	σ (kG)
51 423.462	1500	−67	10	53 004.15871	600	52	18
51 423.478	1200	−98	13	53 004.16712	600	35	14
51 423.493	1200	−105	12	53 004.17582	600	54	12
51 423.508	1200	−122	12	53 004.24442	600	0	13
51 423.523	1200	−116	15	53 004.25570	600	−1	14
51 423.531	900	−102	16	53 004.26512	600	−8	21
51 423.539	600	−108	15	53 005.16007	1500	61	27
51 423.547	600	−112	13	53 006.14914	600	24	13
51 423.554	600	−110	13	53 006.15736	600	49	13
51 423.562	600	−101	12	53 006.16564	600	48	11
53 003.15306	600	84	10	53 006.17401	600	60	11
53 003.16255	600	45	13	53 006.18243	600	54	10
53 003.17105	600	57	18	53 006.19954	600	65	10
53 003.17976	600	34	15	53 006.21667	600	54	10
53 003.18935	600	26	18	53 006.22521	600	37	11
53 003.19806	600	47	13	53 006.23373	600	20	12
53 003.20656	600	50	16	53 006.24227	600	35	12
53 003.21513	600	25	14	53 006.25063	600	8	10
53 003.22362	600	29	18	53 006.25910	600	4	12
53 003.23238	600	58	20	53 006.26747	600	−11	10
53 003.24116	600	15	18	53 006.27362	600	−30	10
53 003.24972	600	22	17	53 006.28170	600	−59	10
53 003.25831	600	−27	18	53 006.29233	600	−56	11
53 003.26672	600	−32	16	53 006.30086	600	−89	23
53 003.27531	600	−51	15	53 006.30889	600	−69	12
53 003.28373	600	−14	15	53 007.14476	600	75	10
53 003.29223	600	−74	18	53 007.15302	600	55	10
53 003.30066	600	−53	16	53 007.16151	600	54	10
53 003.30921	600	−113	16	53 007.17095	600	60	10
53 003.31784	600	−91	18	53 007.18220	600	65	11
53 003.32629	600	−112	14	53 007.19011	600	68	12
53 003.33477	600	−133	14	53 007.19797	600	44	11
53 003.34319	600	−124	14	53 007.20591	600	65	10
53 003.35171	600	−135	15	53 007.21409	600	50	10
53 003.36033	600	−101	14	53 007.22229	600	33	10
53 003.36896	600	−101	13	53 007.23095	600	9	12
53 003.37737	600	−108	15	53 008.13248	600	39	13
53 003.38564	600	−67	18	53 008.14073	600	25	10
53 003.39399	600	−55	16	53 008.14909	600	54	15
53 003.40234	600	−72	12	53 008.15723	600	59	11
53 003.41075	600	−55	15	53 008.16522	600	63	13
53 003.41914	600	−20	17	53 008.17352	600	43	13
53 003.42765	600	5	19	53 008.18212	600	78	14
53 003.43626	600	9	21	53 008.19032	600	66	15
53 003.47535	1800	60	28	53 008.19842	600	71	14
53 004.12513	600	48	13	53 008.20713	600	39	12
53 004.13348	600	20	16	53 008.21590	600	39	12
53 004.14188	600	61	13	53 008.22407	600	48	13
53 004.15034	600	60	18				

Fig. 1. Power spectrum the magnetic field variations of WD 0009+501 (*upper plot*) and cleaned spectrum (*lower plot*) for the main sinusoidal signal $P \approx 8$ h.

Finally, our previous observations (Fabrika et al. 2003), together with the data from Schmidt & Smith (1994) made it possible to further test the realibity of our estimate of the rotation period. A combined analysis of the measurements with the data of Fabrika et al. (2003) and Schmidt & Smith (1994) confirmed that the best fit is obtained adopting a rotation period of about 8 h. The magnetic phase curve of WD 0009+501 derived with this period is presented in Fig. 2. The phase curve is almost sinusoidal and symmetrical about the value of about -30 kG. The longitudinal magnetic field varies from -120 ± 10 kG to $+50 \pm 5$ kG.

The period derived is in good agreement with all other available observations. For the maximum of the mean longitudinal field we calculate the following ephemeris:

$$JD = 2\,453\,003.34 \pm 0.005 + 0\overset{d}{.}334 \pm 0.008\,E.$$

4. Phase resolved *I* and *V* Stokes spectra. Determinations of mean longitudinal field, mean field modulus, and crossover

After the determination of the rotation period via analysis of the B_l measurements, we combined spectra using four consecutive exposures obtained at two orthogonal orientations of the quarter-wave plate (the sequence of its position angles is $+45°, -45°, -45°, +45°$). The resulting combined exposures correspond to a total of 600 s integration time as logged in Table 1. From these spectra, we obtained individual Stokes *I* and *V* by applying the technique presented by Naydenov et al. (2002; see also Aznar Cuadrado et al. 2004). Finally, we build phase-resolved Stokes *I* and *V* spectra by further combining individual Stokes *I* and *V* spectra into 20 phase bins
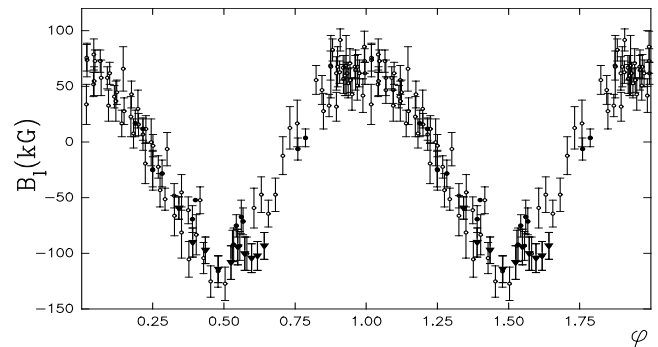

Fig. 2. The magnetic phase curve of WD 0009+501 with the 8-h period. Empty circles indicate the new observations presented in this paper, filled circles are observations by Schmidt & Smith (1994) and triangles are the data by Fabrika et al. (2003).
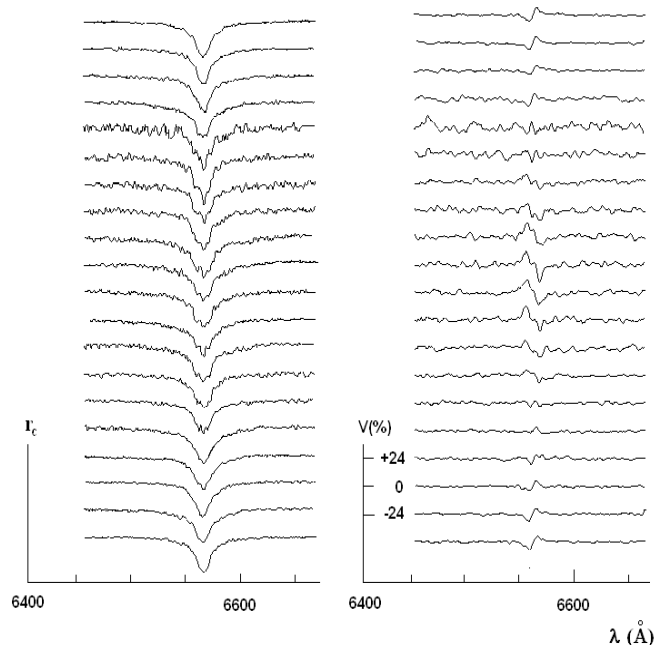

Fig. 3. Phase-resolved Stokes *I* (*left*) and Stokes *V* (*right*) profiles of WD 0009+501 in the Hα region phased with the period $P = 8$ h and binned in 0.05 ϕ intervals. The rotation phase increases from bottom to top, $\phi = 0$ corresponds to the B_l maximum.

taken 0.05 apart. In all cases, the coadditions of individual Stokes *I* and *V* profiles was performed weigthing the individual spectra with coefficients that depend on the noise.

The final Stokes *I* and *V* profiles are presented in Fig. 3. The rotation phase in the figure increases from bottom to top, $\phi = 0$ corresponds to maximum B_l. The magnetic variablility of the Hα Stokes *V* profile is clearly seen.

Figure 4 shows the Hα profile in three specific phases: $\phi = 0$ (the maximum field $B_l \approx 50$ kG), the crossover (zero B_l) and $\phi = 0.5$ (the minimum field $B_l \approx -120$ kG). The resolved Zeeman triplet at the moment of the minimum field provides the most reliable estimate of the surface magnetic field at this point: about 300 kG.

An initial inspection of the data did not reveal any evidence of important non-dipolar field components requiring a more
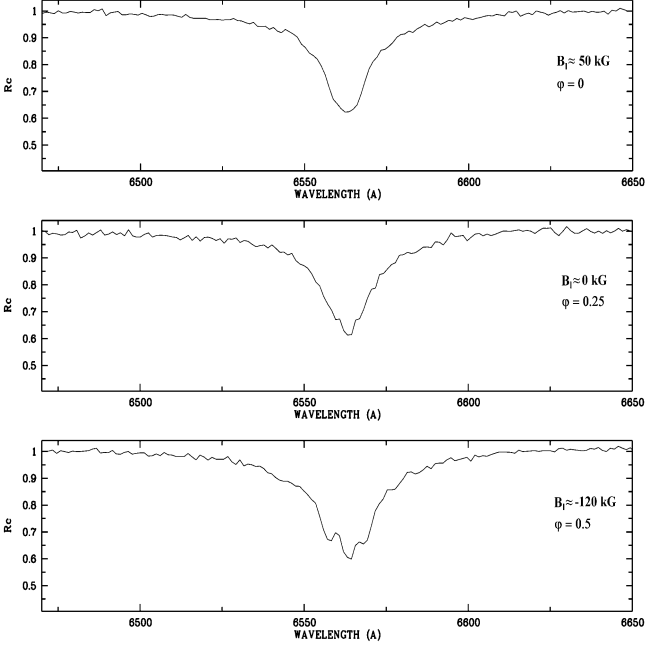
Fig. 4. Hα line profiles of WD 0009+501 (*from top to bottom*) in the maximum magnetic field ($B_l \approx 50$ kG), the crossover and in the minimum field ($B_l \approx -120$ kG).

sophisticated analysis using Zeeman tomography (e.g. Euchner et al. 2002). The Stokes V spectra show a single S-shaped profile which changes sign during the stellar rotational cycle, indicative of a dominant dipolar component in the field. For this reason we do not model the detailed Stokes V profiles, but consider the data in terms of mean observables obtained from the spectra: mean longitudinal field, surface field and crossover. Despite the fact that individual measurements of magnetic observables are only weakly sensitive to higher-order field components, these components can be detected by analysing the phase variation of the observables (Bagnulo et al. 2002). In order to perform a more detailed analysis of the Stokes V profiles, higher signal-to-noise ratios are required.

4.1. Mean longitudinal field determinations

From the Stokes I and V profiles, binned in 0.05-cycle intervals, we have obtained the longitudinal field determinations through the expression

$$V(\lambda) \sim B_l \left(\frac{\lambda}{\lambda_0}\right)^2 \frac{1}{I_\lambda} \frac{dI_\lambda}{d\lambda}, \qquad (2)$$

where $\frac{dI_\lambda}{d\lambda}$ describes the flux profile, λ_0 is a Balmer line rest wavelength (see Angel et al. 1973; also Schmidt & Smith 1995, and references therein).

The measurements are presented in Cols. 2 and 3 of Table 2, and plotted in the upper panel of Fig. 5. The longitudinal magnetic field shows almost sinusoidal variability with minor (but statistically significant) deviations. Using a first order Fourier expansion, $B_l = A + B \sin(2\pi t/P + \phi_0)$ the best-fit was obtained with the parameters $A = -23 \pm 2$ kG, $B = 77 \pm 3$ kG (see thin solid lines in the top panel of Fig. 5).

Table 2. WD 0009+501: phase-resolved observable magnetic quantities longitudinal field, mean field modulus or "surface field", and crossover.

Rot. phase	B_l (kG)	$\sigma(B_l)$ (kG)	B_s (kG)	$\sigma(B_s)$ (kG)	$v_e \sin i \langle dB_z \rangle$ (kG km s^{-1})	$\sigma(v_e \sin i \langle dB_z \rangle)$ (kG km s^{-1})
0.025	+49	6	190	16	−90	80
0.075	+42	5	163	18	−69	70
0.125	+25	7	169	15	+58	70
0.175	+17	9	155	15	+250	65
0.225	−4	8	138	13	+32	100
0.275	−11	7	187	14	+25	130
0.325	−52	9	200	19	−78	150
0.375	−73	14	228	18	−360	230
0.425	−99	15	254	20	+540	260
0.475	−119	14	259	23	+13	235
0.525	−125	15	258	18	−178	190
0.575	−105	14	288	22	−380	220
0.625	−71	14	255	20	−641	260
0.675	−63	9	300	30	−425	320
0.725	−18	14	245	50	+47	300
0.775	0	16	250	75	−208	580
0.825	+35	11	205	35	−182	80
0.875	+42	6	191	17	+100	90
0.925	+48	5	200	15	−47	65
0.975	+53	4	181	15	+168	70

4.2. Mean field modulus determinations

The spectral resolution ($R \sim 2000$) also makes it possible to estimate a surface magnetic field B_s at each phase bin. (The surface field is the modulus $|B|$ of the total magnetic vector integrated over the star's visible hemisphere.) To measure B_s we used estimative method based on deblending of the line core by means of simultaneous fit of three Gaussian profiles. Such a method makes it possible to reconstruct Zeeman pattern at each point of the phase curve and estimate the surface field by measurements of the displacement of the Gaussians. The measurements are presented in Cols. 4 and 5 of Table 2, and plotted in the middle panel of Fig. 5.

4.3. The second-order moment of the Hα Stokes V profile: crossover determinations

We have attempted to measure the second order moment in phase-resolved Stokes V spectra of the Hα profile, namely the quantity

$$R_V^{(2)} = \frac{1}{W(H\alpha)} \int V(\lambda)(\lambda - \lambda_0)^2 d\lambda. \qquad (3)$$

Mathys (1995) has shown that $R_V^{(2)}$ is an estimate of the so called mean asymmetry of the longitudinal field multiplied by $v_e \sin i$, the crossover $v_e \sin i \langle dB_z \rangle$. Unfortunately, our observations are characterized by a *S/N* ratio that is too low to determine the crossover with sufficiently high precision. Integration
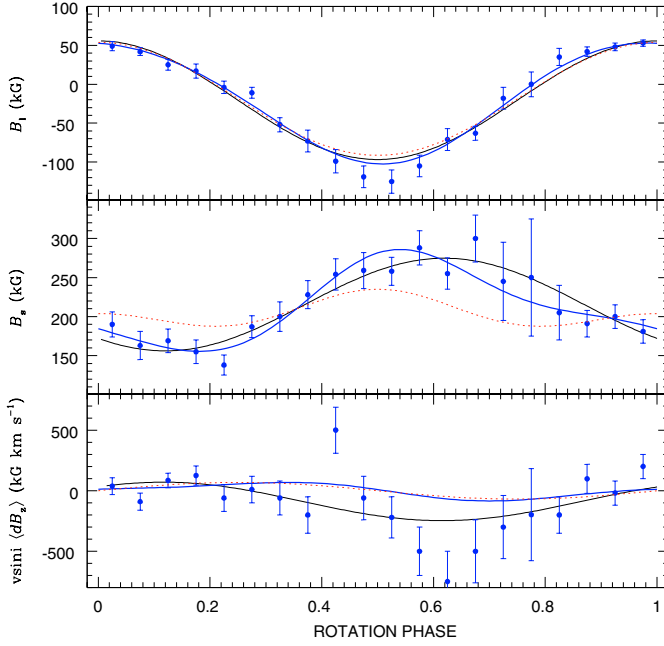
Fig. 5. Observations and modelling of mean longitudinal field (*top panel*), mean field modulus, or surface field (*middle panel*) and crossover (*bottom panel*). The thin solid lines show a fit obtained with simple second order Fourier expansion. Thick solid lines show the best-fit obtained by means of a dipole + quadrupole model. Dotted lines show the best-fit obtained assuming that a simple dipole model.

of Stokes V in the wings of the Hα profile leads to very large error bars of $R_V^{(2)}$ because the noise grows as a quadratic function of the distance from λ_0 (the larger the spectral line width, the larger the impact of the error on Stokes V to the final error bar on $R^{(2)}$). We therefore decide to integrate $V(\lambda)(\lambda - \lambda_0)^2$ only in central Hα regions where the Stokes V parameter is significantly different from zero (typically ± 30 Å from the Hα core). Such a way one may affect the result toward over- or underestimation of the second order moment. Nevertheless, we find it helpful to present the data here and use them in our consideration as a first illustration for the magnetic white dwarfs. The measurements are presented in Cols. 6 and 7 of Table 2, and plotted in the bottom panel of Fig. 5.

5. Modelling the magnetic field of WD 0009+501

It is generally assumed that the magnetic morphology of white dwarfs is organized at a large scale, and that can be possibly described by means of a low-order multipolar expansion (Putney 1999). To quickly see if the observations of WD 0009+501 are consistent with a simple dipolar geometry, we have followed the schematic method proposed by Landolfi et al. (1997). Inspection of Fig. 5 shows that i) the mean field modulus curve has only two extrema (case I A of Eq. (6) of Landolfi et al. 1997); ii) the mean field modulus at phase 0 is smaller than the mean field modulus at phase 0.5, (case II B of Eq. (8) of Landolfi et al. 1997). Finally,

iii) $B_l^{max} > 0 > B_l^{min}$, $|B_l^{max}| < |B_l^{min}|$,

(case 4 III of Eq. (4) of Landolfi et al. 1997). A comparison with Table 1 of Landolfi et al. (1997) shows that these features,

all together, are *not* consistent with a pure dipolar configuration. Therefore we have decided to model the measurements of mean longitudinal field, mean field modulus, and crossover of Table 2 within the framework of a dipole plus quadrupole field as defined in Landolfi et al. (1998). The modelling technique is described in detail in Bagnulo et al. (2000). Here we recall that the curves of mean longitudinal field, surface magnetic field, and crossover, are interpreted in terms of a dipole plus quadrupole model. The best-fit to the observations is obtained through a Marquardt method of χ^2 minimisation (Bevington 1969). The dipole plus quadrupole model depends on the following 10 parameters:

– B_d and B_q, the dipole and quadrupole strength, respectively;
– v_e, the stellar equatorial velocity;
– i, the inclination of the stellar rotation axis to the line of sight;
– β, the angle between the dipolar axis and the rotation axis;
– β_1 and β_2, the analogues of β for the directions identified by the quadrupole;
– γ_1 and γ_2, the azimuthal angles of the unit vectors of the quadrupole;
– f_0, the "reference" rotational phase of the model.

The angles i, β, β_1, β_2 range from 0° to 180°, while γ_1, γ_2, f_0 range from 0° to 360°. The rotational period P and the limb-darkening constant u, which also affects the expressions of the magnetic observables, are taken as fixed. (Note that the pure dipole model would retain as free parameters only B_d, v_e, i, β, and f_0.)

For the stellar mass, Wickramasinghe & Ferrario (2000) estimated the value of $0.89 M_\odot$, which approximately corresponds to a stellar radius of $0.009 R_\odot$ (Hamada & Salpeter 1961). Finally, for this work, we decided to set as a constraint $R/R_\odot = 0.01 \pm 0.002$.

Based on our low resolution spectra, we are not able to set a strong constraint on $v_e \sin i$. However, introducing our radius and period estimate in the formula

$$v_e \sin i \le \frac{50.8 R/R_\odot}{P(\text{d})} \text{ km s}^{-1},$$

we obtain that $v_e \sin i$ must be less than 2 km s^{-1}.

For the limb-darkening coefficient, we adopted the value of $u = 0.5$. Note that, as discussed by Bagnulo et al. (2000), the results of the modelling are only slightly influenced by the u value. The best-fit parameters are:

i	=	60°	±	20°
β	=	111°	±	17°
f_0	=	0°	±	3°
β_1	=	52°	±	35°
β_2	=	104°	±	27°
γ_1	=	331°	±	37°
γ_2	=	178°	±	40°
B_d	=	338	±	70 kG
B_q	=	278	±	208 kG
v_e	=	1.53	±	0.15 km s^{-1}

and the associated $v_e \sin i$ and radius values are 1.32 ± 0.40 km s^{-1} and $0.010 \pm 0.001 R_\odot$, respectively.

Note that, as explained by Bagnulo et al. (2000), the available observations do not allow one to distinguish between two magnetic configurations symmetrical about the plane containing the rotation axis and the dipole axis. Such configurations are characterised by the same values of B_d, B_q, v_e, γ_1, γ_2, f_0, while the remaining angles are related by

$$(i, \qquad \beta, \qquad \beta_1, \qquad \beta_2)$$
$$(180° - i, \ 180° - \beta, \ 180° - \beta_1, \ 180° - \beta_2).$$

The best-fit to the observations is shown with solid lines in Fig. 5. For comparison, the dotted line shows the best-fit obtained using a simple dipolar morphology. The parameters of the best dipole model are

i	=	63°	±	24°
β	=	117°	±	24°
f_0	=	1°	±	2°
B_d	=	295	±	6 kG
v_e	=	1.50	±	0.15 km s^{-1}

and the associated $v_e \sin i$ and stellar radius values are 1.34 ± 0.25 km s^{-1} and 0.010 ± 0.001 $R_\odot$, respectively. It is worthwhile to note that the dipole parameters are very similar in both models, whereas the quadrupolar component of the dipole+quadrupole model is left quite undetermined due to the large error bars.

The detection of a significant quadrupolar component is not a big surprise. Returning back to our previous observations of WD 0009+501 (Fabrika et al. 2003) we note that the (wrong) estimate of 2 h for the rotational period was based on the analysis of observations obtained in a 2.5 interval, during which the star showed negative longitudinal field. In Fabrika et al. (2003), our observations of a noise bimodal structure around the negative extremum of the field had been erronesouly interpreted as the modulation due to a full rotation cycle. In fact, the observed bimodal structure (that is washed out in the rebinning of the data) could possibly be the signature of field structure even more complex than a dipole plus quadrupole.

6. Conclusions

We have presented new observations of low-resolution Stokes I and V profiles of the magnetic white dwarf WD 0009+501. From these and previous observations we have determined the star's rotation period, we have determined the mean longitudinal field, the mean field modulus, and the crossover. Finally we have developed a magnetic model consistent with all the observations.

The rotation period of WD 0009+501 is 0.334 ± 0.008 d, based on our new observations as well as archival data obtained by Fabrika et al. (2003) and Schmidt & Smith (1994).

The longitudinal magnetic field of WD 0009+501 varies from −120 ± 10 kG to +50 ± 5 kG. The surface field shows a variation between ≈150 and ≈300 kG.

Assuming the magnetic field of WD 0009+501 to be a dipole we found its basic parameters: the rotation axis inclination is about 60° and the dipole axis inclination about 120°; the field strength at the pole, B_d, is about 295 kG. However,

it is clear from the fit to the observations that the dipole model is not sufficient to explain all available observations.

Assuming the magnetic field of WD 0009+501 is given by the superposition of a dipole and quadrupole, we found that the rotation axis inclination is about 60° and the dipole axis inclination about 110°; the polar field of the dipole $B_d \approx 340$ kG; the quadrupole field B_q of about 300 kG. The orientation of the dipolar angles are almost the same as obtained under the assumption of a pure dipolar model, but the quadrupole configuration is left quite undetermined because of the large error bars associated to the model parameters.

Landstreet & Mathys (2000) have discovered that slow rotating magnetic Ap stars (i.e. with rotation period of about 1 month or longer) have a magnetic axis tilted at a small angle with respect to the rotation axis. Landstreet & Mathys (2000) and Bagnulo et al. (2002) suggest also that faster rotating stars tend to have a magnetic axis that forms a large angle with the rotation axis. Taking into account fairly short rotation period of the degenerate we may hypothesize that white dwarf magnetic fields display similar correlations with rotational period as those of the magnetic Ap/Bp stars. According to Landstreet & Mathys (2000), long-period magnetic Ap/Bp stars exhibit small magnetic tilt angles (i.e. magnetic axes nearly aligned with rotational axes), whereas short-period Ap/Bp stars exhibit large tilt angles (i.e. magnetic axes nearly perpendicular to rotational axes). In WD0009+501, we have found that the dipolar axis of the field forms a large angle with respect to the rotational axis. It would be interesting to explore whether the field tilt angle is also correlated with rotational period in the MWDs. If established on a sound statistical basis, this result could imply that there are universal dynamical mechanisms in the magnetic main sequence stars and their remnants worthy of additional study.

Finally, it should be noted that the polar strength of the dipole of WD 0009+501 is about 300 kG. Assuming magnetic flux conservation during MS star evolution into a white dwarf, we estimate that the dipole strength during the star's life on the main sequence was of a few tens of Gauss. This implies that either Ap stars with extremely weak dipole fields exist (which is not supported by the results of Auriere et al. 2004, who find that all Ap stars have dipole fields stronger than about 300 G), or that a significant flux loss occurs during the post-main sequence evolutionary processes, or that stars other than magnetic chemically peculiar Ap/Bp stars evolve into magnetic white dwarfs. The last assumtion has been recently supported by Wickramasinghe & Ferrario (2005). They argue that magnetic white dwarfs have progenitors that are not restricted to Ap/Bp magnetic stars. To address these issues, further studies of weak-field white dwarfs are needed.

References

Afanasiev, V. L., Burenkov, A. N., Vlasyuk, V. V., & Drabek, S. V. 1995, SAO Ras internal Rep., 234

Angel, J. R. P., McGraw, J. T., & Stockman, H. S. 1973, ApJ, 184, L79

Angel, J. R. P., Borra, E. F., & Landstreet, J. D. 1981, ApJS, 45, 457

Aznar Cuadrado, R., Jordan, S., Napiwotzki, R., et al. 2004, A&A, 423, 1081

Auriere, M., Donati, J.-F. F., Lignieres, D., et al. 2004, in The A-Star Puzzle, the Proc. IAU Symp., 224, in press

Bagnulo, S., Landolfi, M., Mathys, G., & Landi Degl'Innocenti, M. 2000, A&A, 358, 929

Bagnulo, S., Landi Degl'Innocenti, M., & Landolfi, M. 2002, A&A, 394, 1023

Bevington, P. R. 1969, Data reduction and error analysis for the physical sciences (New York: McGraw-Hill)

Euchner, F., Jordan, S., Beuermann, K., Gänsicke, B. T., & Hessman, F. V. 2002, A&A, 390, 633

Fabrika, S. N., Valyavin, G. G., & Burlakova, T. E. 2003, Astron. Lett., 29, 737

Goransky, V. 2004, private communication

Hamada, T., & Salpeter, E. E. 1961, ApJ, 134, 683

Klochkova, V. G., Yermakov, S. V., & Panchuk, V. E. 1996, Bull. Spec. Astrophys. Obs., 41, 58

Lafler, J., & Kinman, T. D. 1965, ApJS, 11, 216

Landolfi, M., Bagnulo, S., Landi Degl'Innocenti, E., Landi Degl'Innocenti, M., & Leroy, J. L. 1997, A&A, 322, 197

Landolfi, M., Bagnulo, S., & Landi Degl'Innocenti, M. 1998, A&A, 338, 111

Landstreet, J. D., & Mathys, G. 2000, A&A, 359, 213

Liebert, J., Bergeron, P., & Holberg, J. B. 2003, AJ, 125, 348

Mathys, G. 1995, A&A, 293, 733

Maxted, P. F. L., Ferrario, L., Marsh, T. L., & Wickramasinghe, D. T. 2000, MNRAS, 315, L41

Monin, D. N., Fabrika, S. N., & Valyavin, G. G. 2002, A&A, 396, 131

Muslimov, A. G., Van Horn, H. M., & Wood, M. A. 1995, ApJ, 442, 758

Naydenov, I. D., Valyavin, G. G., Fabrika, S. N., et al. 2002, Bull. Spec. Astrophys. Obs., 53, 124

Putney, A. 1999, 11th European Workhop on White Dwarfs, ed. J. E. Solheim, & E. G. Meistas, ASP Conf. Ser., 196, 195

Scargle, J. D. 1989, ApJ, 343, 874

Schmidt, G. D., & Smith, P. S. 1994, ApJ, 423, L63

Schmidt, G. D., & Smith, P. S. 1995, ApJ, 448, 305

Terebizh, V. 1992, Analysis of time rows in astrophysics, in Russian (Nauka: Moscow)

Valyavin, G. G., Burlakova, T. E., Fabrika, S. N., & Monin, D. N. 2003, Astron. Rep., 47, 589

Wade, G. A., Bagnulo, S., Szeifert, T., et al. 2003, in Solar Polarization, ed. J. Trujillo Bueno, & J. Sánchez Almeida, ASP Conf. Ser., 307, 565

Wendell, C. E., Van Horn, H. M., & Sargent, D. 1987, ApJ, 313, 284

Wickramasinghe, D. T., & Ferrario, L. 2000, PASP, 112, 873

Wickramasinghe, D. T., & Ferrario, L. 2005, MNRAS, 356, 1576